Journal of Computer-Aided Molecular Design (2020) 34:983–1002
https://doi.org/10.1007/s10822-020-00318-w

# Computational exploration and experimental validation to identify a dual inhibitor of cholinesterase and amyloid-beta for the treatment of Alzheimer's disease

**Manish Kumar Tripathi[1] · Piyoosh Sharma[1] · Avanish Tripathi[1] · Prabhash Nath Tripathi[1] · Pavan Srivastava[1] · Ankit Seth[1] · Sushant Kumar Shrivastava[1]**

Received: 11 November 2019 / Accepted: 26 May 2020 / Published online: 3 June 2020


## Abstract

The cholinesterases are essential targets implicated in the pathogenesis of Alzheimer's disease (AD). In the present study, virtual screening and molecular docking are performed to identify the potential hits. Docking-post processing (DPP) and pose filtration protocols against AChE and BChE resulted in three hits (AW00308, HTS04089, and JFD03947). Molecular Mechanics-Generalized Born Surface Area (MM-GBSA) and molecular dynamics simulation analysis affirmed the stability and binding pattern of the docked complex JFD03947, which was further synthesized and evaluated for in vitro cholinesterase inhibition (AChE, $IC_{50} = 0.062$ μM; BChE, $IC_{50} = 1.482$ μM) activity. The enzyme kinetics study of the JFD03947 against hAChE and hBChE suggested a mixed type of inhibition. The results of thioflavin T-assay also elicited anti-Aβ aggregation activity by JFD03947. Further, biological evaluation of identified compound JFD03947 also showed neuroprotective ability against the SH-SY5Y neuroblastoma cell lines.

**Keywords** Molecular docking · Molecular dynamics · Virtual screening · Acetylcholinesterase · Butyrylcholinesterase · Anti-Aβ aggregation

## Introduction

Alzheimer's disease (AD) is one of the most fearsome, sophisticated, and age-associated neurodegenerative disorder, which is the most common cause of dementia [1–3]. It is characterized by the decline in cognitive abilities [4], mood swings, loss of memory [5], disorientation, difficulties with language, and behavioral changes [6, 7]. It is one of the significant public health issues with its maximum prevalence in developing countries, especially in the elderly population [8]. It is a multifactorial disease that creates a high social and economic burden worldwide [9, 10].

In the past decades, several hypotheses have been proposed to be involved in AD. Among them, the cholinergic hypothesis is the most common, which describes the degeneration of cholinergic neurons in the brain [11, 12]. The loss of ACh and subsequently altered cholinergic neurotransmission adversely affects the human cognitive functions and causes memory alterations [13]. This hypothesis suggests that the cognitive functions may be improved by enhancing the ACh levels or by inhibiting its hydrolysis [14]. To augment cholinergic neurotransmission, the inhibition of acetylcholinesterase (AChE) is an essential therapeutic strategy [15–18]. At present, there are only four drugs in the market to treat this challenging disorder. Among those, three are AChE inhibitors (donepezil, rivastigmine, and galantamine), and an NMDA receptor antagonist (memantine). All these drugs are reported for symptomatic relief in the AD [16], and they are inefficacious in disease modification [19].

Among available drugs, rivastigmine also acts on another cholinesterase named butyrylcholinesterase (BChE), which has 65% structural similarity to AChE along with functional

**Electronic supplementary material** The online version of this article (https://doi.org/10.1007/s10822-020-00318-w) contains supplementary material, which is available to authorized users.

✉ Sushant Kumar Shrivastava
skshrivastava.phe@iitbhu.ac.in

[1] Pharmaceutical Chemistry Research Laboratory, Department of Pharmaceutical Engineering & Technology, Indian Institute of Technology (Banaras Hindu University), Varanasi 221005, India

similarities [20]. This enzyme exists in the central and peripheral nervous system, in most tissues, along with intestine, lungs, pancreas, and liver [21]. The inhibition of BChE is also reported to enhance memory and cognition. Investigations also confirmed the involvement of BChE in AD patients having progressive loss of ACh [22, 23]. Several clinical evidence suggested that BChE also plays a significant role in the regulation of ACh in maintaining the normal cholinergic functions in AD [24, 25]. The activity of BChE was observed to be elevated during AD [26–28]. Therefore, inhibition of AChE and BChE can be considered as a potential therapeutic advantage in the advanced and late phase of AD.

AD is a multifaceted disorder interrelated with complex pathogenic mechanisms like, i.e., decreased level of ACh, deposition of amyloid β (Aβ), tau protein, and oxidative stress [29]. The role of AChE is also reported to induce Aβ formation resulting in the highly toxic AChE-Aβ peptide complex [30]. The outer gorge of AChE, known as peripheral anionic binding site (PAS) that is rich in hydrophobic amino acid residues, has the property to stimulate the Aβ aggregation [31]. Thus, AChE inhibitors that interact exclusively with the peripheral anionic site (PAS) also helps in enhancing the cholinergic transmission and prevent the pro-aggregating activity of AChE toward Aβ. These multiple factors in AD pathology need to develop and discover novel scaffolds of next-generation, which could be useful in disease-modifying therapy by acting through dual inhibition and reduce the formation of neurotoxic aggregates.

The purpose of this study is based on computational explorations of the Maybridge Hit finder database containing 14,400 compounds to identify novel hits targeting cholinesterases (AChE and BChE). Virtual screening protocols were employed to screen potential hits that interact with active site residues of both the enzymes. The identified ligands with respective docked poses were screened by Molecular Mechanics-Generalized Born Surface Area (MM-GBSA), molecular dynamics, and drug likeliness prediction studies. The previous findings intrigued us to synthesize the top hit (JFD03947), which is characterized by physicochemical and spectral techniques and evaluated for dual ChE inhibition (AChE and BChE). Further, its potential for neurotoxicity and Aβ aggregation inhibition was also evaluated.

## Materials and methods

### Computational studies

#### Protein preparation and grid generation

Briefly, 3D crystal structures of AChE (PDB Code: 4EY7, *Homo sapiens*) and BChE (PDB Code: 6EYF, *Homo sapiens*) complexes were retrieved for this study. Protein Preparation Wizard module of the Schrödinger suite was used to prepare respective protein crystal structures [32]. Structures were processed by removal of water molecules, addition of hydrogen atoms, filling of missing side chains and loops, followed by restraining minimization, and structure refinement using the OPLS force field [33]. Grids were prepared using the Protein Grid Generation module by defining the box volume of 10 × 10 × 10 Å surrounding active sites of the respective co-crystallized ligands. The prepared grids and docking protocol were validated by extracting and re-docking co-crystallized ligands in respective grid structures. Superposition tool was used to compare and calculate the RMSD of actual and re-docked poses of a co-crystallized ligands for AChE and BChE.

#### Selection and preparation of ligands

The chemical database of Maybridge Hit finder (http://www.maybridge.com/) containing 14,400 compounds (accessed in October 2018), was used for screening and identifying potential inhibitors. The downloaded ligands were optimized, and minimum energy conformers were generated by LigPrep module of the Schrödinger 2018-1 using default parameters at pH 7.4.

#### Structure-based virtual screening

The virtual screening protocols were accomplished using the Glide module, and potential hits were identified from the generated conformers of ligands. Hierarchal filtration protocols were used to determine the best possible binding poses in the receptor grid space. A three-stage filter screening process was used: (i) high throughput virtual screening (HTVS), (ii) standard precision (SP), and (iii) extra precision (XP) docking with filtration criteria of 10%, 20%, and 25% in each successive steps, respectively [34]. Further, the identified poses were analyzed by docking-post processing and pose filtration protocols. Common potential hits against AChE and BChE were identified and processed for further studies.

#### Binding free energy calculation

MM-GBSA Prime Module of Schrödinger 2018-1 was used to evaluate the binding affinity of identified docked complexes [35]. The Prime module uses XP docked "out.maez" file and rank the ligands based on the calculated binding energy. The equation used by the prime module to calculate binding energy is

$$\Delta G_{binding} = G_{complex} - (G_{protein} + G_{ligand})$$

where $G_{complex}$, $G_{protein}$, and $G_{ligand}$ are optimized free energies of the complex, free protein, and free ligand, respectively.

#### In silico drug likeliness characteristics

The QikProp module of the Schrödinger 2018-1 was used to predict the drug likeliness characteristics of identified potential hits. Some important properties were predicted, such as molecular weight, numbers of hydrogen bond donors and acceptors, total solvent accessible surface area (SASA), brain/blood partition coefficient (QPlogBB), log of octanol/water partition coefficient (QPlogPo/w), apparent Caco-2 cell permeability (QPPCaco), apparent MDCK cell permeability (QPPMDCK), binding to human serum albumin (QPlogKhsa), and Lipinski's rule of five.

#### Molecular dynamics simulations

In the drug discovery process, the molecular dynamics simulation is widely used for microscopic examination of protein-ligand interactions in an explicit water environment. Desmond module of Schrödinger Maestro 2018-1 was used for molecular dynamics simulation, and runs of 100 ns timescale were performed to affirm the binding stability of docked poses of AW00308, HTS04089, and JFD03947 on both AChE and BChE. The docked complexes of donepezil with AChE and rivastigmine with BChE were also simulated, and obtained results were used for comparative assessment. Using the system builder option of Desmond, each docked complexes were soaked adequately in the TIP3P water molecules through the orthorhombic water box [36]. The systems were further neutralized by adding the counterions and minimized by steepest descent and LBFGs algorithm using maximum 2000 iterations with convergence criteria of 1 kcal/mol/Å. After the system minimization, the production run of molecular dynamics was carried out with the periodic boundary condition, a constant number of atoms (N), pressure (P) and temperature (T) NPT ensemble, the temperature at 300K and 1.013 bars atmospheric pressure. The non-bonded interaction was computed at the truncation distance of 9 Å, Particle mesh Ewald (PME) method was used to calculate electrostatic interaction. The recording interval energy and trajectories were set to 1.2 ps and 50 ps, respectively. Finally, the molecular dynamics simulation run of docked complexes were performed for 100 ns. The generated trajectories after complete production runs were used to generate simulation interaction diagrams, and the results were analyzed.

## Chemistry: synthesis and characterization

All reagents and solvents used in the studies were procured from commercial sources and used without further purification. FT-IR spectrum was recorded on Bruker ECO-ATR (Alpha). $^{1}$H NMR (500 MHz) and $^{13}$C NMR (125 MHz) spectra were performed using Avance Bruker FT-NMR spectrometer in DMSO-$d_6$ using TMS as an internal standard.

#### Synthesis of JFD03947

The ethanolic solution of 1,4-bis(aminomethyl)cyclohexane (*cis*- and *trans*-mixture) (**1**) (1 mmol) and 2-hydroxybenzaldehyde (**2**) (2 mmol) with 2–3 drops of glacial acetic acid were refluxed for 4 h. The solution was allowed to cool at room temperature to afford the solid compound, which was recrystallized from absolute ethanol to get pure compound JFD03947 [37].

Yield: 72.8%, Yellow solid; FT-IR ($cm^{-1}$): 1606 (–HC = N), 3460 (–OH); $^{1}$H NMR (500 MHz, DMSO-$d_6$) δ 1.42–1.54 (m, 6H), 1.76–1.81 (m, 3H), 3.34–3.57 (m, 5H, $–CH_2–N=$), 6.85–6.90 (m, 4H), 7.30–7.44 (m, 4H), 8.53 (d, 2H, $J$ = 16 Hz), 13.75 (s, 2H); $^{13}$C NMR (125 MHz, DMSO-$d_6$) δ 26.50, 30.48, 36.61, 62.47, 117, 118.84, 119.00, 132.05, 132.71, 161.42, 166.36. Anal. $C_{22}H_{26}N_2O_2$: C, 75.40; H, 7.48; N, 7.99; Found: C, 75.64; H, 7.42; N, 7.86.

## Biological evaluation of selected compound

#### In vitro cholinesterase inhibition assay (hAChE and hBChE)

Ellman assay was performed to determine the ChE inhibitory potential of target compounds JFD03947 [38]. The hAChE stock solution (EC No. 3.1.1.7, from human erythrocytes) was prepared in HEPES buffer (20 mM; pH 8) and Triton X-100 (0.1% v/v). The hBChE (EC No. 3.1.1.8, from human serum) stock solution was prepared in aqueous gelatine solution (0.1% w/v). The five increasing concentrations of test compounds were prepared in DMSO that preferably causes 20–80% inhibition (final concentration ≤ 1% v/v). Initially, a test compound (10 µL) was pre-incubated for 10 min with a stock solution of hAChE or hBChE (25 µL; 0.25 U/mL), followed by the addition of 340 µM 5,5-dithio-bis-(2-nitrobenzoic acid) (DTNB), and 550 µM of ATCI and BTCI as a substrate for hAChE & hBChE respectively. The blank readings were taken with all the components except enzyme to account for the nonenzymatic hydrolysis of substrates. The change in absorbance was recorded at 37 °C for 6 min (wavelength = 412 nm) on Multimode Reader (BioTek Synergy H1M, USA). The rate of the reactions with or without inhibitors was compared, followed by the measurement of percentage inhibition using the following expression: $[(V_o - V_i)/V_o] \times 100$, where $V_i$ is the rate of reaction with

inhibitor and $V_o$ is the reaction rate without inhibitor. The $IC_{50}$ value of JFD03947 was calculated by non-linear variable slopes of log (inhibitor) *vs* normalized response (Graph Pad Prism 5.01) [39]. The assay was performed in triplicate.

Enzyme kinetics study was performed for JFD03947 at six varied concentrations of ATCI or BTCI (66–400 µM) to determine the nature of inhibition of hAChE and hBChE. Three different concentrations of the compound JFD03947 (0.030, 0.060, 0.090 µM for hAChE; and 1.0, 1.5, 2.0 µM for hBChE) were taken for the experiment and evaluated against all the six varied concentrations of substrates. The Lineweaver-Burk double reciprocal plot was constructed between varied substrate concentrations and rates of reaction to identify the type of hAChE or hBChE inhibition [40]. Finally, the Ki values were measured by generating the Dixon plots [41]. The assay was performed in triplicate.

#### Aβ aggregation inhibition by thioflavin T assay

Test compound JFD03947 was evaluated for their inhibitory potential against Aβ fibril formation by Thioflavin-T assay [42]. The stock solution of Aβ (2000 µM) was prepared by dissolving the protein in ammonium hydroxide (pH ≥ 9.0). The test compound was prepared in PBS (pH 7.4) and a small quantity of DMSO (≤ 1% w/v) to dissolve the compound. The test compound and Aβ were screened in three different ratios, i.e., 10:5, 10:10, and 10:20 µM, respectively. The experiment was performed in triplicate.

For anti-Aβ aggregation assay, the mixture of Aβ (10 µL, final concentration: 10 µM) in PBS pH 7.4 with or without inhibitor (10 µL, final concentrations: 5 µM, 10 µM, and 20 µM) was incubated (37 °C, 48 h) followed by addition of thioflavin T (180 µL, 5 µM) solution in 50 mM glycine–NaOH buffer pH 8.0. The fluorescence intensity was measured at excitation (λex = 450 nm) and emission (λem = 485 nm) wavelengths. The anti-Aβ aggregatory potential was calculated as percentage inhibition following an expression: [100 – (Fi/Fo × 100)]; and NFI = Fi/Fo. The Fi and Fo are the fluorescence intensities with or without inhibitor, respectively.

#### Neuroprotective studies on SH-SY5Y cell lines

The neurotoxic liability of test compound JFD03947 on SH-SY5Y neuroblastoma cell lines was determined by MTT assay [43]. The protocol of the study was according to literature with slight modification. Condition and medium of cell lines (density $1 \times 10^5$ cells/wells) were seeded on 96 well plates and incubated for 24 h at 37 °C in a humidified atmosphere with 5% $CO_2$. After incubation, cells were exposed to compound JFD0397 at varying concentrations (10, 20, 40, and 80 µM) and incubated at 37 °C for 24 h. After incubation, the media containing test compounds were replaced with fresh media and treated with Aβ (20 µM), followed by incubation for another 24 h at 37 °C. In each well, 20 µL (5 mg/mL) of MTT reagent was added, and the cells were incubated for 3 h. The MTT media was discarded and obtained purple-colored formazan crystals were solubilized in solvent (100 µL 0.1 N HCl in isopropanol). The absorbance was measured at 570 nm, and the % cell viability was calculated. Each treatment was executed in triplicate, and data are presented as a percentage of the control.

The overall workflow used for the hit identification and validation is given in Fig. 1.

## Results

### Computational studies

#### Virtual screening and hit identification

The virtual screening workflow of the Schrödinger Maestro 2018-1 was used to screen Maybridge hit finder database compounds (14,400 compounds) based on their affinity for the binding site of cholinesterase enzymes. Docking protocols and prepared grids of enzymes were validated to avoid the false-positive results of molecular docking. Re-docking with co-crystallized ligands was performed in the generated grid. Further, the superposition tool was used to align actual pose with the docked pose of the respective ligands. RMSD has often been used to measure the quality of reproduction of a known (i.e., crystallographic) binding pose by a computational method, i.e., docking. The RMSD value was found within the range of less than 2.0 Å, which represented a good and correct pose. Reported literature suggested that RMSD value under 2.0 Å are significant and acceptable [44, 45]. Thus, the obtained results validated our docking protocol.

The virtual screening workflow selectively filters the ligands based on their potential to interact with the target structure. All the generated conformers 18,930 were screened using virtual screening methods. Based on the Glide scoring protocol, 95 potential hits were identified for both the targets and processed for docking-post processing and pose filtration.

#### Docking-post processing and pose filtration

The 3D crystal structures of AChE and BChE revealed that active site of AChE and BChE containing five subsites, namely, CAS, PAS, oxyanion hole, acyl binding pocket, and anionic subsite [28, 46]. The CAS, PAS, and Anionic subsite amino acid residues were considered as most important for the functionality of enzymes. Thus, the hits showing interaction with the CAS (His447 for AChE and His438 for BChE), PAS (Trp286 for AChE and Asp70 for BChE) and Anionic subsite (Trp86, Phe338 for AChE and Trp82, Glu197, Ala

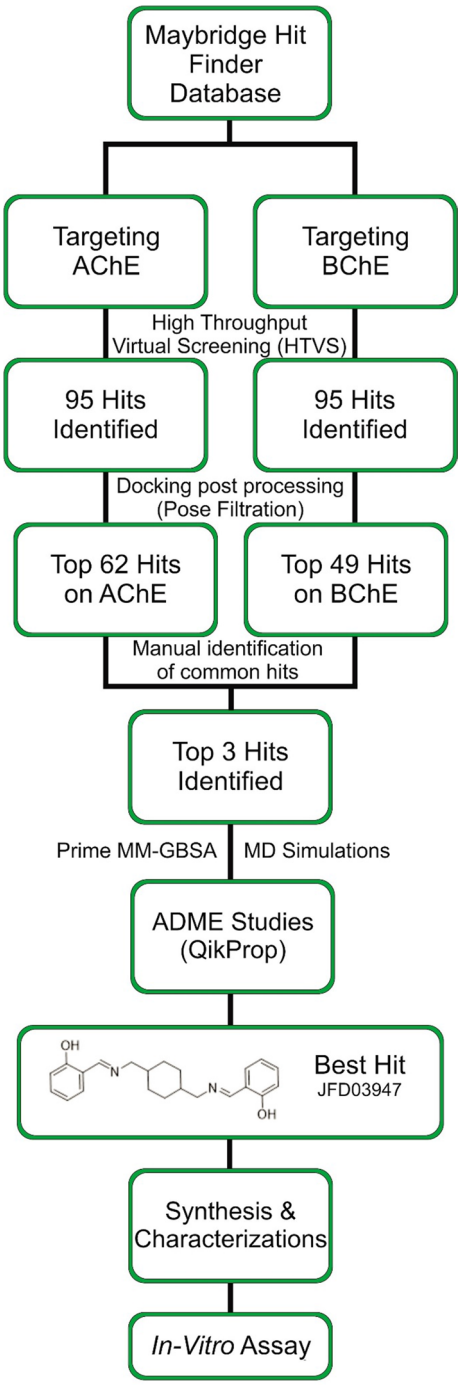


**Fig. 1** Flowchart of the proposed methodology

328 for BChE) were selected as the leading filtration criterion to choose out the significant pose (60 hits for AChE and 45 hits for BChE) of compounds (Supplementary Tables S1 and S2).

The common hits amongst the screened ligands interacting with both the enzymes at CAS, PAS, and anionic subsite were manually identified, and the compounds AW00308, HTS04089, and JFD03947 were found as the common hits (Fig. 2).

### Binding mode elucidation of hits identified by virtual screening (VS)

**Binding mode analysis of AW00308** Binding mode analysis of AW00308 with PAS of AChE showed the interaction of phenyl ring with amino acid residues Tyr72, Tyr124, Trp286, and Tyr341 under the hydrophobic pocket. Trp286 also showed π–π interaction with the phenyl ring. Whereas Asp74 amino acid residue of the PAS region showed electrostatic interaction with the phenyl moiety of AW00308. The docked pose of donepezil also showed a similar type of interaction in the PAS site (Fig. S1). The nitrogen atom of the piperazine ring in identified hit interacted with an anionic subsite Phe338 and Trp86 amino acid residues through hydrophobic and π–cation interaction. In CAS, His 447 and Ser203 showed charged interaction with the pyrimidine ring, comparable to the donepezil where benzyl piperazine moiety, also showed the charged interaction. In anionic subsite, phenyl ring showed hydrophobic interaction with Phe295 and Phe297 residues (Fig. 3a, b). These interactions are similar to the donepezil except for the PAS residue. Phe295 showed both hydrophobic and hydrogen bonding interactions in donepezil, whereas the AW00308 showed hydrophobic interaction only (Fig. S1).

The binding mode analysis of AW00308 with BChE revealed that allylic hydroxy showed hydrogen bonding with His438 residues at CAS. Rivastigmine moiety also showed a similar hydrogen-bonding pattern with His438 residue. At the acyl binding pocket, the phenyl ring showed hydrophobic interaction with Leu286 and Phe329 residue. Pyrimidine moiety showed polar interaction with Glu197 and hydrophobic interaction with Trp82 amino acid residue. In the PAS region, Asp70 showed charged interaction with phenyl ring, and Tyr332 showed hydrogen bonding with the nitrogen atom of piperazine moiety of the compound. Dimethyl ethanamine moiety of rivastigmine also showed charged interaction with Asp70 and hydrogen bonding interaction with Tyr322 amino acid of the PAS site. (Fig. 3c, d).

**Binding mode analysis of HTS04089** The binding mode of HTS04089 was evaluated with both the targeted enzymes. At the PAS site of AChE, the compound interacted with Tyr74, Tyr124, Trp286, and Tyr341 through hydrophobic interactions with the 2-methoxyphenyl moiety. Tyr341 also formed π–π stacking interaction with this moiety. In the donepezil docked complex similar to HTS04089 hydrophobic interaction was showed by 1,4 indonale-1,1 moiety with Tyr341, and this moiety also formed π–π stacking interaction with Trp286 residue (Fig. S1). Whereas, Asp74 amino acid of the PAS region showed charge interaction with the

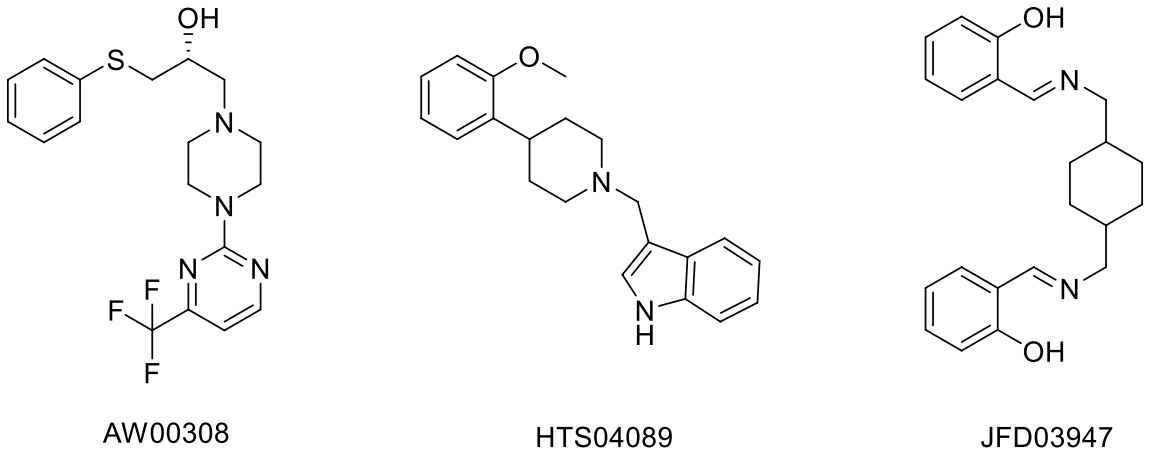


**Fig. 2** 2D structures of identified hits

2-methoxyphenyl moiety and hydrophobic interaction with Phe295 and Phe297 amino acid residues of an acyl binding pocket. The nitrogen atom of the piperidine ring formed the π–π stacking and π cation interaction with the anionic subsite Trp86 residue, whereas the piperidine ring showed hydrophobic interaction with the Trp86 and Phe338 residue. The indole ring of the identified lead showed polar interaction with His447 and Ser203 amino acid residue at CAS comparable to the benzyl piperazine moiety of donepezil (Fig. 4a, b).

The binding analysis of HTS04089 with CAS of BChE revealed that the nitrogen atom of the indole ring showed charged and hydrogen bonding interaction with His438. These similar interactions were identified in the CAS region, identical to the rivastigmine docked pose. At PAS, Asp70 amino acid interacted with the nitrogen atom of piperidine ring by hydrogen bonding and showed a charged interaction, whereas 2-methoxyphenyl ring showed hydrophobic interaction with Tyr332. Dimethyl ethanamine moiety of rivastigmine also showed the same hydrogen bonding and hydrophobic interaction pattern with Asp70 and Tyr332 amino acid residue. The same interaction pattern was found at anionic subsite. The indole ring showed π cationic interaction and π–π stacking interaction with Trp82 residue, whereas the piperidine ring showed hydrophobic interaction with Ala328 amino acid residue (Table 1). At the acyl binding pocket, amino acids Phe329 showed hydrophobic interaction with the piperidine ring. (Fig. 4c, d).

**Binding mode analysis of JFD03947** The binding mode of JFD03947 on AChE showed very promising results at the CAS, His447, and Ser203 showed charged interaction with o-hydroxy benzylidine similar to the benzyl piperazine moiety of donepezil, which showed charged interaction with CAS residues. 1,4,Di-bis methylamine moiety of JFD03947 was found to be actively involved in hydrophobic interactions with anionic subsite amino acid residues Trp86 and Phe338. Trp86 also showed π–π stacking and π–cation interaction with o-hydroxy benzylidine moiety. A similar interaction pattern was also observed in donepezil, where Trp86 showed hydrophobic and π–π stacking interaction with benzyl piperazine moiety and π–cation interaction with the piperazine moiety. This moiety also showed hydrophobic and π–cation interaction with the Phe338 residue (Figs. S1, S2).

Interaction pattern of JFD03947 with acyl binding pocket amino acid residues Phe295 and Phe297 showed hydrophobic interaction with the o-hydroxy benzylidine moiety similar to the 1,4 indonale-1,1 moiety of donepezil docked complex interaction, which showed hydrogen bonding and hydrophobic interactions with Phe295 and Phe297 amino acid residues (Fig. S1). The oxygen atom of o-hydroxy benzylidine moiety also formed hydrogen bonding with Phe295 amino acid residue. The active site residues of the PAS region Tyr124, Trp286, and Tyr341 showed hydrophobic interaction with JFD03947 (Fig. 5a, b).

The docked pose of JFD03947 at BChE revealed that it formed the polar interaction with His438 residues of the CAS site, while rivastigmine showed charged interaction. The JFD03947 showed charged, and the dimethyl ethanamine moiety of rivastigmine also showed salt bridge interactions with Asp70 and hydrophobic interaction with Tyr332 were observed in both rivastigmine and JFD03947 at PAS. Further, *o*-hydroxybenzylidine moiety of JFD03947 showed their interaction with Trp82 amino acid residues through π–π stacking and π–cation interaction and hydrogen bonding with Glu197 amino acid residues. Ala328 amino acid residue showed hydrophobic interaction with the anionic subsite similarly to the rivastigmine (Table 1). The benzylidine ring was also involved in hydrophobic interactions with Val288 and Phe329 at an acyl binding pocket (Fig. 5c, d).

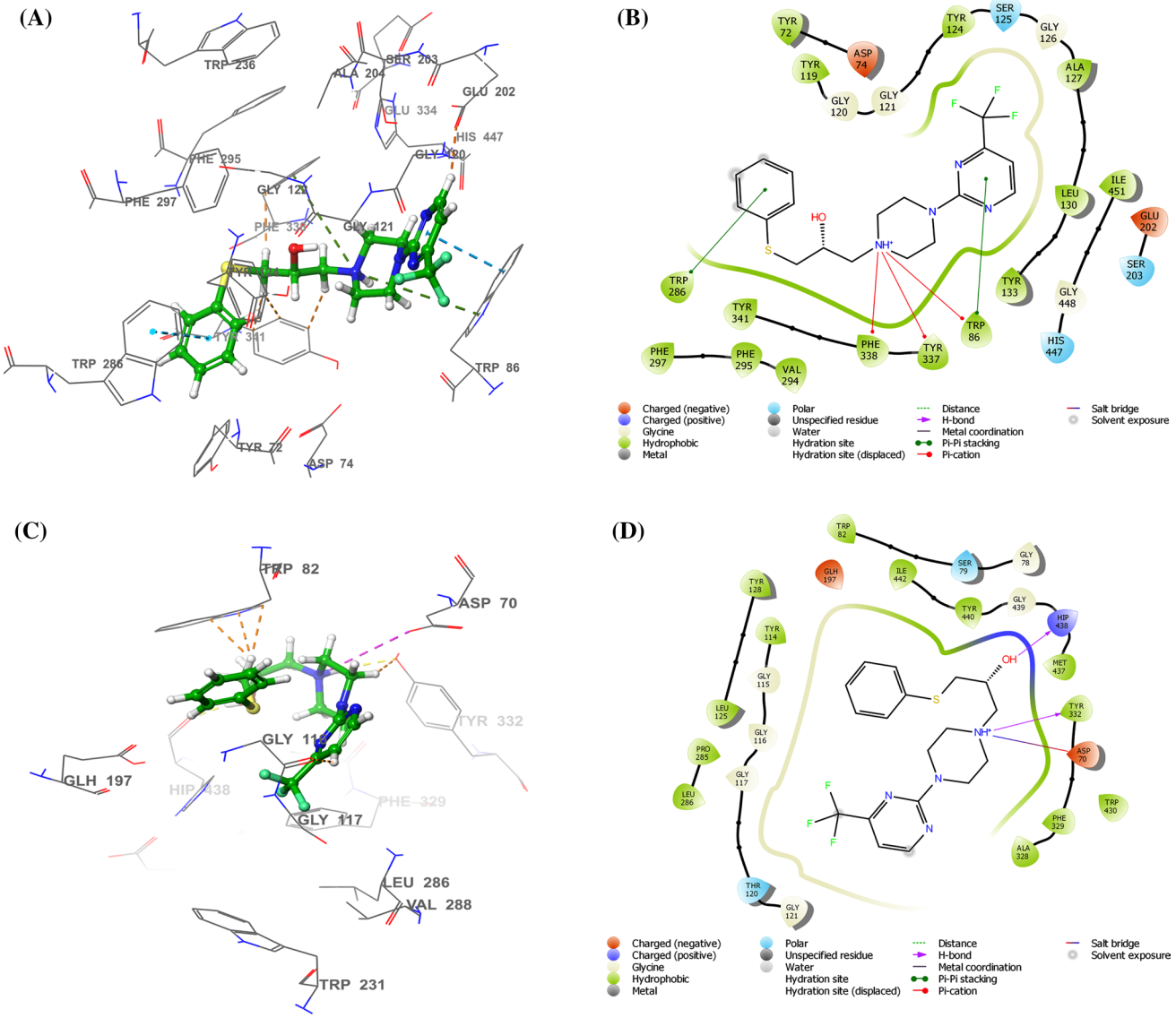


**Fig. 3** In silico molecular docking simulations analysis of AW00308 on AChE (4EY7) and BChE (6EYF) **a** 3D docked pose of AW00308 with AChE; **b** 2D docked pose of AW00308 with AChE; **c** 3D docked pose of AW00308 with BChE; **d** 2D docked pose of AW00308 with BChE

### Binding free energy calculation using Prime/MM-GBSA

The binding energies of the docked protein-ligand complexes for all three hits along with standards (Donepezil and Rivastigmine) were evaluated using the prime MM/GBSA module of Schrödinger 2018-1. The JFD03947 showed minimum ΔG binding energy score for both the enzyme complexes (AChE, ΔG = − 89.23 kcal/mol and BChE, ΔG = − 79.19 kcal/mole). The details of ΔG bind score of all the compounds are shown in Table 1. The docking score of JFD03947 was found to be relatively similar to the donepezil and rivastigmine on AChE and BChE, respectively.

### In silico estimation of drug likeliness properties

Drug-likeliness characteristics for identified hits were predicted using the QikProp module of Schrödinger Maestro 2018-1. The predicted outcomes of some important parameters are reported in Table 2. From the calculated parameters, Qplog Po/w, which predicts the partition coefficient revealed that all compounds (AW00308 = 4.09, HTS04089 = 4.78, and JFD03947 = 4.65) showed higher lipophilicity compared to standard donepezil (4.25). QPPCaco provided the prediction of gut-blood barrier transportation abilities using Caco-2 cells. The results exhibited excellent permeability for all the compounds. The predicted QPlogKhsa values

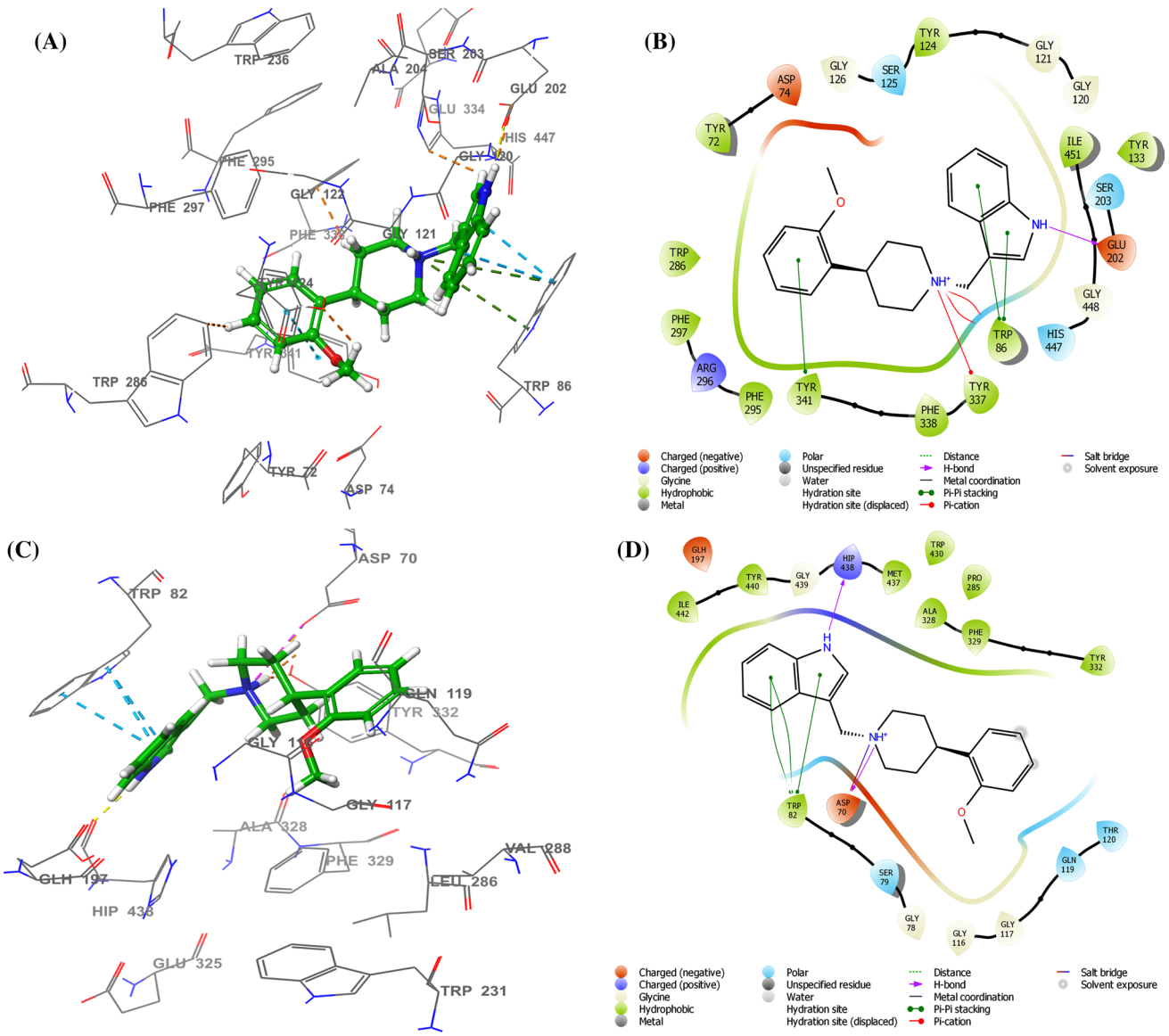


**Fig. 4** In silico molecular docking simulations analysis of HTS04089 on AChE (4EY7) and BChE (6EYF) **a** 3D dock pose of HTS04089 with AChE; **b** 2D dock pose of HTS04089 with AChE; **c** 3D dock pose of HTS04089 with BChE; **d** 2D dock pose of HTS04089 with BChE

affirmed their strong binding with plasma protein. The outcome of Lipinski's rule of five (MW < 500, QPlog Po/w < 5, donorHB 0–6.0, acceptHB 2.0–20), along with the other predicted parameters indicated that the investigated compounds elicited "drug-like" characteristics, which were comparable with standard drug.

### Molecular dynamics simulation of selected hits identified from VS

The molecular dynamics simulation runs of 100 ns were performed to evaluate the stability and flexibility of the docked complexes on AChE and BChE enzymes. Six simulation systems were run independently for three identified hits (AW00308, HTS04089, JFD03947) complex with AChE (PDB Code: 4EY7) [47] and BChE (PDB Code: 6EYF) [48]. We also performed the 100 ns simulation to the docked complexes of donepezil with AChE and rivastigmine with BChE to compare the results with identified hits. The 100 ns time scale was enough for the side-chain rearrangement in the native as well as the docked complexes to gain the most stable binding conformation. The residual fluctuations in the target proteins were determined by the root mean square deviations (RMSD) and root mean square fluctuations (RMSF) protocols. The analysis of interacting residues was evaluated to predict the binding behavior in a docked pose during MD simulation.

**Table 1** Results of molecular docking, interacting residues and binding free energies

| S. No. | Enzyme | Compound ID | Glide Score[#] | Interacting residues* | | | ΔG binding energy[†] |
|---|---|---|---|---|---|---|---|
| | | | | CAS | PAS | Other active sites | |
| 1 | AChE (4EY7) | AW00308 | − 14.35 | His447[a]<br>Ser203[a] | Tyr341[c]<br>Trp286[c,e]<br>Tyr124b[c]<br>Tyr72[c]<br>Asp74[f] | Trp86[c,d,e]<br>Phe295[c]<br>Phe297[c]<br>Phe 338[c,d] | − 48.29 |
| | | HTS04089 | − 15.01 | His447[a]<br>Ser203[a] | Tyr341[c,e]<br>Trp286[c]<br>Tyr124[c]<br>Tyr72[c]<br>Asp74[f] | Trp86[c,e]<br>Phe295[c]<br>Phe297[c]<br>Phe 338[c] | − 53.64 |
| | | JFD03947 | − 16.74 | His447[a]<br>Ser203[a] | Tyr341[c]<br>Trp286[c]<br>Tyr124[c] | Trp86[c,d,e]<br>Phe295[b,c]<br>Phe297[c]<br>Phe 338[c] | − 89.23 |
| | | Donepezil | − 14.6 | His447[a]<br>Ser203[a] | Tyr341[c]<br>Trp286[c,e]<br>Tyr124[c]<br>Tyr72[c]<br>Asp74[f] | Trp86[c,d,e]<br>Phe295[b,c]<br>Phe297[c]<br>Phe338[c,d] | − 59.06 |
| 2 | BChE (6EYF) | AW00308 | − 7.15 | His438[b,f] | Asp70[f,g]<br>Tyr332[b,c] | Trp82[c]<br>Leu286[c]<br>Phe329[c]<br>Ala328[c]<br>Glu197[f] | − 69.28 |
| | | HTS04089 | − 8.37 | His438[b,f] | Asp70[b,f]<br>Tyr332[c] | Trp82[c,e]<br>Phe329[c]<br>Ala328[c]<br>Glu197[f] | − 65.09 |
| | | JFD03947 | − 5.58 | His438[f] | Asp70[f,g]<br>Tyr332[c] | Trp82[c,d,e]<br>Val288[c]<br>Phe329[c]<br>Glu197[b,f]<br>Ala328[c] | − 79.19 |
| | | Rivastigmine | − 4.9 | His438[b,f] | Asp70[f]<br>Tyr332[b,c] | Trp82[c]<br>Leu286[c]<br>Val288[c]<br>Trp231[c]<br>Phe329[c,d]<br>Ala199[a]<br>Ala328[c]<br>Glu197[f] | − 39.32 |

[#]Glide scores were calculated in kcal/mol. Glide XP visualizer module was used to analyze the docked poses; [†]binding free energy (kcal/mol) was calculated using the molecular mechanics-generalized born surface area (MM/GBSA); *all interactions were observed in the range of 4 Å radius between the ligands and interacting residues

Types of interactions: [a]polar; [b]H-bonding; [c]hydrophobic; [d]π–π cation; [e]π–π stacking; and [f]electrostatic interaction; [g]salt bridge

The structural stability of the docked complexes was assessed by the RMSD pattern of all the docked complexes. The results revealed that all the docked complexes have stable trajectories throughout the simulation time scale with average fluctuations in the range of 1–3 Å (Fig. 6a, b). In AChE docked complexes, RMSD value showed a sharp increase up to 15 ns after with fluctuations to be maintained within the acceptable range. These observations suggested that AChE and its docked complexes reached the equilibrium states along with structural stability during the simulation. The RMSD backbone of the AChE protein was found to be stable during the entire simulation time. Moreover, The RMSD value for the AChE–JFD03947 complex was found to have lesser fluctuations as compared to other simulation systems after 15 ns. Thus, small fluctuations in the entire simulation time scale of AChE–JFD03947 complex indicated that flexibility of AChE was declined and the complex was found to be relatively stable. The comparative

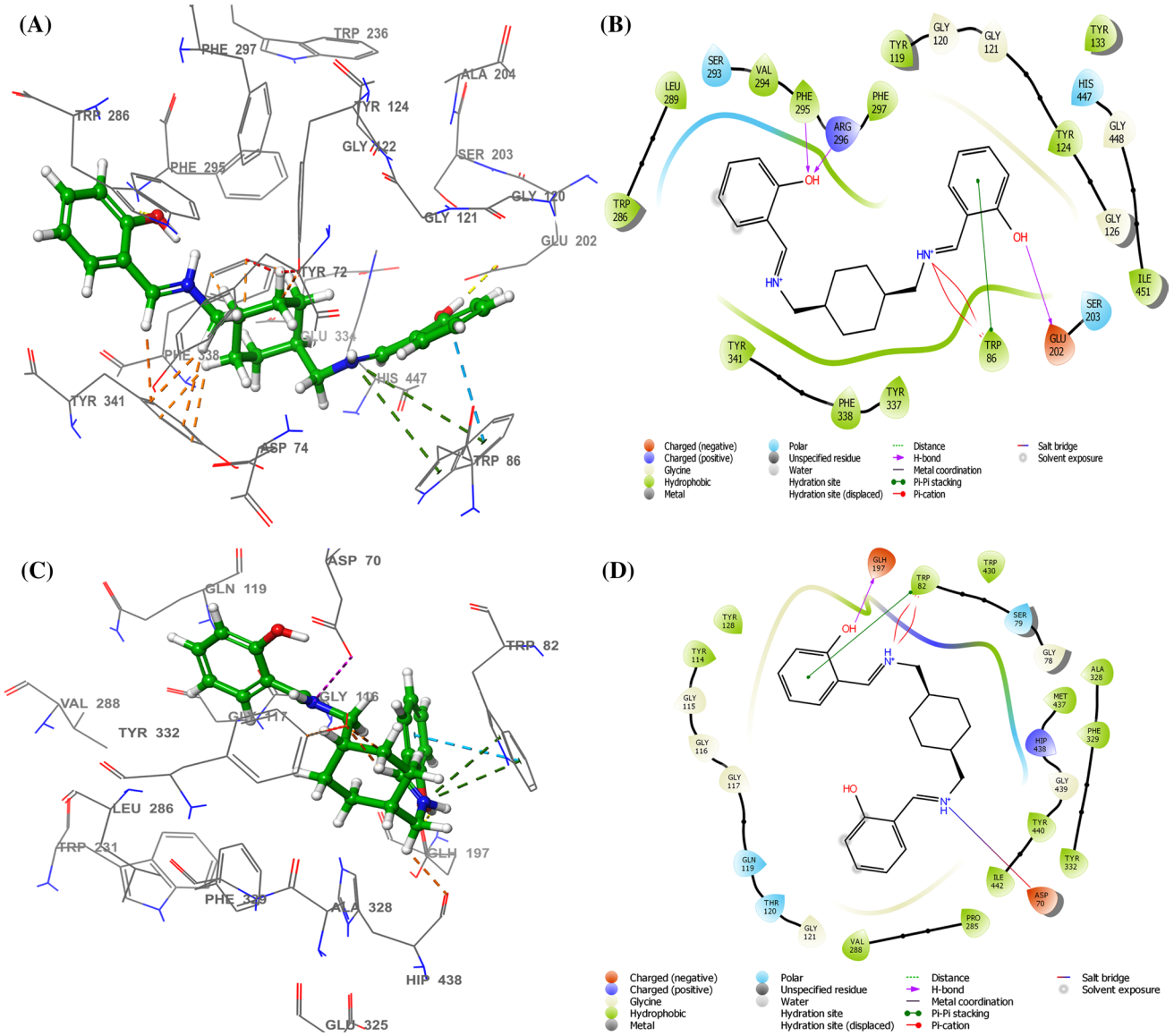


**Fig. 5** In silico molecular docking simulations analysis of JFD03947 on AChE (4EY7) and BChE (6EYF) **a** 3D dock pose of JFD03947 with AChE; **b** 2D dock pose of JFD03947 with AChE; **c** 3D dock pose of JFD03947 with BChE; **d** 2D dock pose of JFD03947 with BChE

simulation results JFD03947 and Donepezil with docked complexes showed similar RMSD behavior and fluctuation patterns. The RMSD patterns of other docked complexes (AW00308, HTS04089) showed the larger fluctuations behavior during the entire simulation time than donepezil, which inferred that docked complexes were not stable during the simulation time scale. In the BChE simulation system, trajectories of the other two systems showed larger fluctuations except for the BChE–JFD03947 complex (Fig. 5b). The BChE-JFD03947 docked complex trajectory was found to be stable and showed fewer variations within the acceptable range of RMSD values. The stability and fluctuation behavior of JFD03947 was also found to be comparable to the rivastigmine docked complex in BChE. Further, a comparison of trajectories between docked complexes of AW00308, HTS04089 with rivastigmine inferred larger fluctuation during the entire simulation time and their trajectories were also not found to be in the range of the acceptable region. The RMSF values were calculated using Cα atoms of the enzymes to get insights into the structural fluctuations of active amino acid residues due to the presence of ligand. The RMSFs were evaluated for the CAS and PAS active site residues and found to be stable for all the enzyme-ligand complex systems (Fig. 7a, b).

The results of interaction analysis were performed using the Simulation Interaction Diagram module of Desmond in Schrodinger Maestro 2018-1. The interaction analysis was performed using stacked bar charts as interaction fractions.

**Table 2** ADME properties of the screened compound

| S. No. | Compound | M. wt | donorHB | acceptHB | SASA | QPlog BB | QPlog Po/w | QPPCaco | Qpp MDCK | QPlog Khsa | Rule of five[a] | rtvFG |
|---|---|---|---|---|---|---|---|---|---|---|---|---|
| 1 | AW00308 | 398.45 | 1 | 6 | 681.65 | 0.44 | 4.09 | 823.34 | 2823.88 | 0.60 | 0 | 0 |
| 2 | HTS04089 | 320.43 | 1 | 3 | 626.73 | 0.51 | 4.78 | 1329.83 | 744.798 | 0.98 | 0 | 0 |
| 3 | JFD030947 | 350.46 | 2 | 4 | 704.49 | − 1.16 | 4.65 | 1003.66 | 496.67 | 0.60 | 0 | 0 |
| 4 | Donepezil | 393.61 | 1 | 7 | 759.67 | 0.14 | 4.25 | 1080.84 | 595.28 | 0.69 | 0 | 0 |
| 5 | Rivastigmine | 250.34 | 0 | 5 | 553.58 | 0.479 | 2.478 | 1409.6 | 793.2 | 0.142 | 0 | 0 |

*donorHB* H-bond donors (range 0 to 6), *acceptHB* H-bond acceptors (range 2 to 20), *SASA* total solvent accessible surface area in square angstroms using a probe with a 1.4 Å radius (range 300 to 1000 Å), *QPlog BB* predicted brain/blood partition coefficient (range −3 to 1.2), *QPlog Po/w* predicted log of octanol/water partition coefficient (range 2 to 6), *QPPCaco* predicted apparent Caco-2 cell permeability in nm/s. Caco2 cells are a model for the gut-blood barrier (< 25—poor; > 500—great), *Qpp MDCK* Predicted apparent MDCK cell permeability in nm/s. MDCK cells are considered to be a good mimic for the BBB (< 25—poor; > 500—great), *QPlog Khsa* prediction of binding to human serum albumin (range − 1.5 to 1.5), *rtvFG* number of reactive functional groups; the specific groups are listed in the jobname .out file. The presence of these groups can lead to false positives in HTS assays and to decomposition, reactivity, or toxicity problems in vivo (range 0–2)

[a]Number of violations of Lipinski's rule of five (maximum 4)

The graphical representation showed as interaction showing % interactions, and timeline representation as interacting residues.

The interaction analysis of AW00308 ligand on AChE revealed it interacted for the maximum period of the simulation run with the active site of PAS (Tyr124, Tyr341) and anionic subsite (Trp86, Phe338) residues. It was observed that hydrophobic interaction, which was formed with Phe295 and Phe297 at an acyl binding pocket, was lost during the entire simulation. In the CAS region, water bridge interaction was observed with Ser203 and His447 amino acid residues during simulation interaction (Supplementary Figs. S2, S3). Similarly, in BChE, AW00308 showed interactions at PAS (Asp70, Tyr332) and anionic subsite (Trp82) only and not with the CAS and other active site residues (Supplementary Figs. S4, S5). The RMSD trajectories of AW00308 were not found to be stable in the acceptable range and showed greater fluctuations.

The interaction analysis of HTS04089 on AChE revealed that it showed stable interactions with anionic subsite (Trp86 and Phe338), and acyl binding pocket residue (Phe295). In the CAS region, water bridge interactions were observed with His447 amino acid. The other active site interactions, including PAS, were not seen with the HTS04089-AChE complex (see Supplementary Figs. S6, S7). Further, the interaction analysis of HTS04089 on BChE showed interaction at CAS with His438, which was found to be unstable. At the PAS, it showed the interaction with Asp70, anionic subsite with Trp82 and Ala328, and an acyl binding pocket with Phe329 residue. Apart from these interactions, other active site interactions were not observed or negligible, which formed significant interactions in the docking pose (see Supplementary Figs. S8, S9). The RMSD trajectory of HTS04089 on BChE was also not found to be stable and acceptable region like AW00308 hit.

The interaction analysis of JFD03947 on AChE revealed that it showed hydrophobic interactions with anionic subsite residues Trp86 and Phe338 and hydrogen bonding interaction with Glu202 residue. At PAS, JFD03947 also formed hydrophobic interactions with active site residues Tyr72, Tyr124, Trp286, Tyr341, and hydrogen bonding interaction with Asp74 (Figs. 8, 9). In the CAS region, His447 formed stable water bridge interactions during simulation time. Further, interaction analysis of JFD03947 on BChE showed that His438 residue of CAS region formed hydrogen bonding interaction. The interaction analysis also revealed that in the PAS region, Asp70 and Tyr332, both amino acid residues showed hydrogen bonding and hydrophobic interactions. In the anionic subsite, Trp82 also formed hydrophobic interaction (Figs. 10, 11). All the interactions of docked pose binding patterns in JFD03947 with AChE and BChE enzymes were successfully observed for respective interaction during the

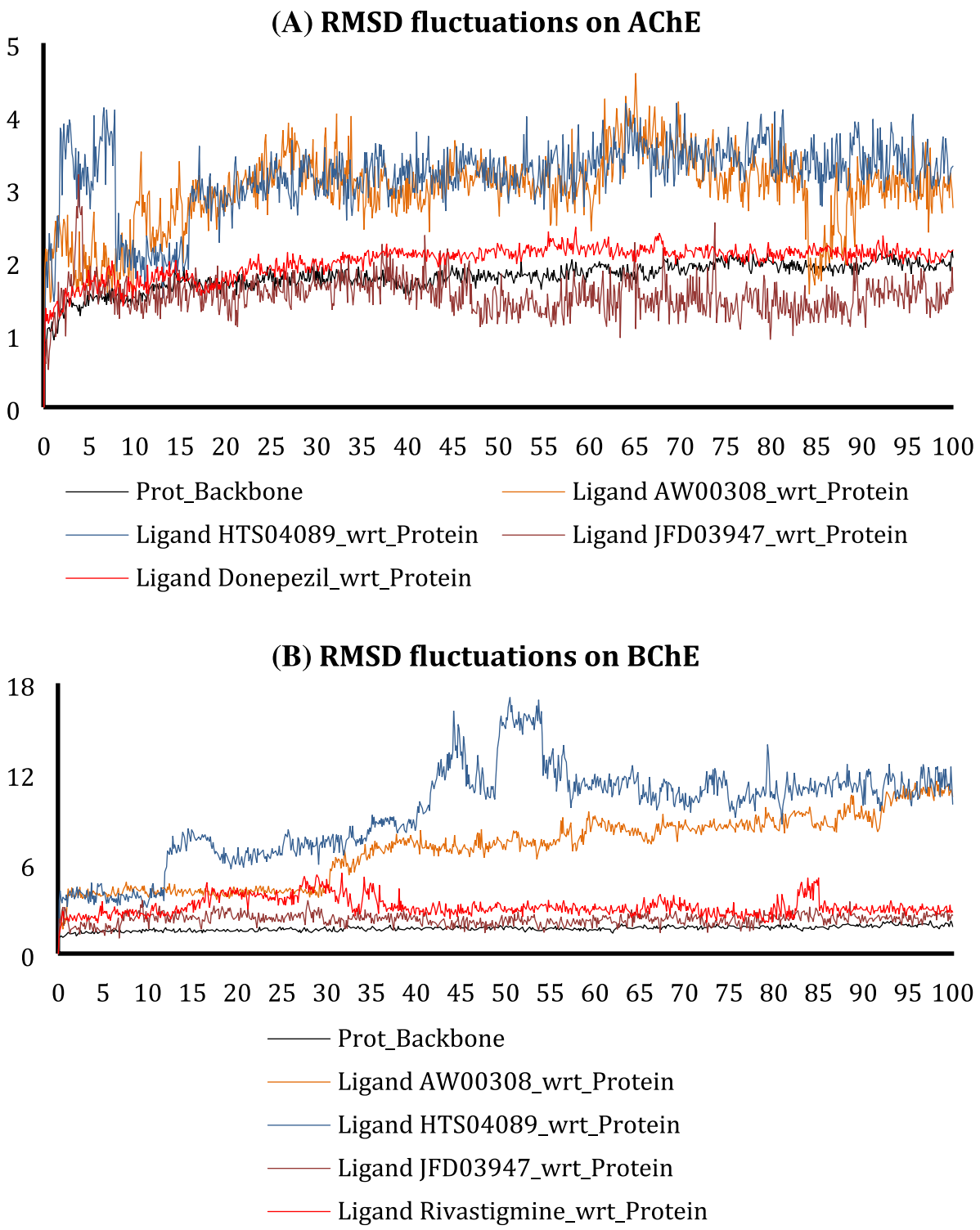


**Fig. 6** RMSD fluctuations of protein backbone (black), AW00308 (orange), HTS04089 (blue), JFD03947 (brown), donepezil (red), and rivastigmine (red) during 100 ns simulation runs on **a** AChE, **b** BChE

molecular dynamics simulation study. The RMSD trajectories of JFD03947 was also found to be stable in both the enzyme system as compare to the other hits like AW00308 and HTS04089.

The interaction analysis of donepezil on AChE revealed stable interaction with PAS (Asp74, Tyr341, Trp286), anionic subsite (Trp86, Phe338), and acyl binding pocket (Phe295, Phe297) (see Supplementary Figs. S10, S11).

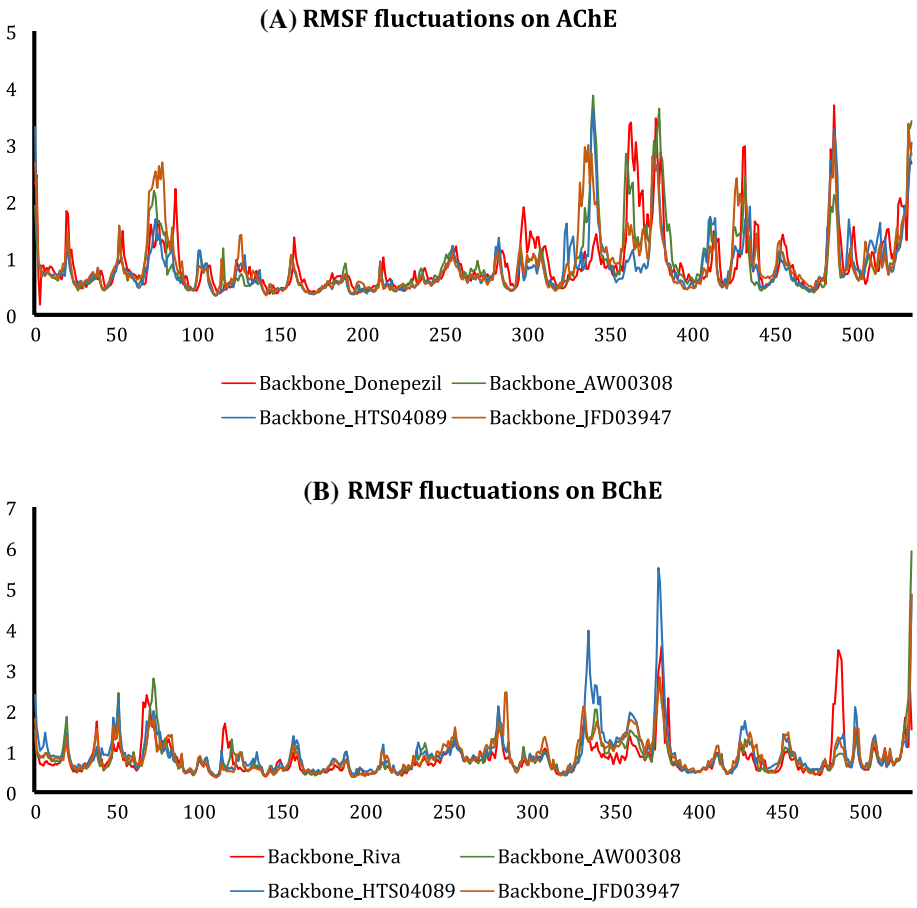


**Fig. 7** Comparative RMSF of **a** AChE and **b** BChE (protein backbone) for top 3 hits in the protein-ligand complex throughout the simulations period of 100 ns.

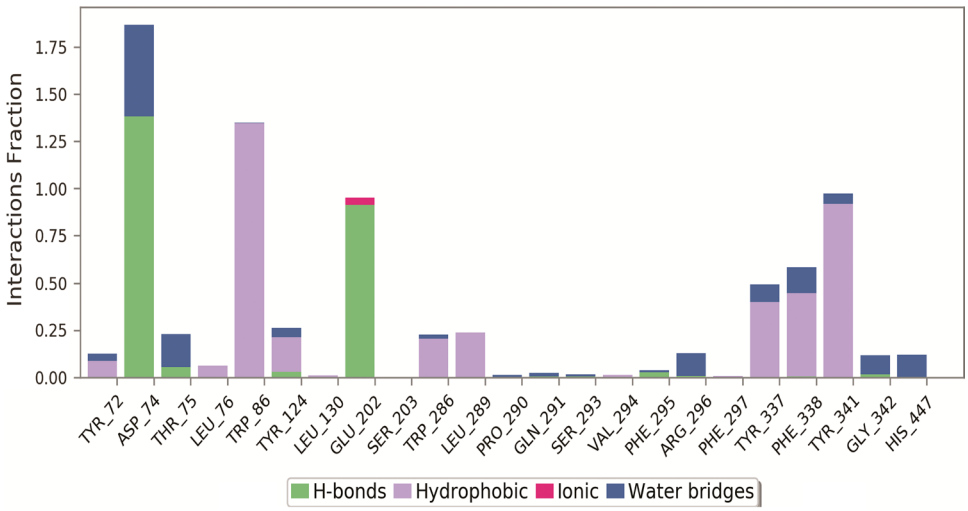


**Fig. 8** Stacked bar chart representation of JFD03947 with active site amino acid residues of AChE

The interaction pattern of rivastigmine during a simulation on BChE revealed hydrogen bonding interaction with CAS residue His438. It also showed stable interaction with PAS (Asp70, Tyr332), acyl binding pocket (Val288, Trp231, Phe329) and anionic subsite (Trp82) residues (see Supplementary Figs. S12, S13). The formed docking interactions were found to be stable in the donepezil and rivastigmine simulations study.

Along with the MM/GBSA calculation, in molecular dynamics simulation studies, RMSD and RMSF protocol were found to be in favor of JFD03947 against both the targets (AChE and BChE). The other hits (AW00308,

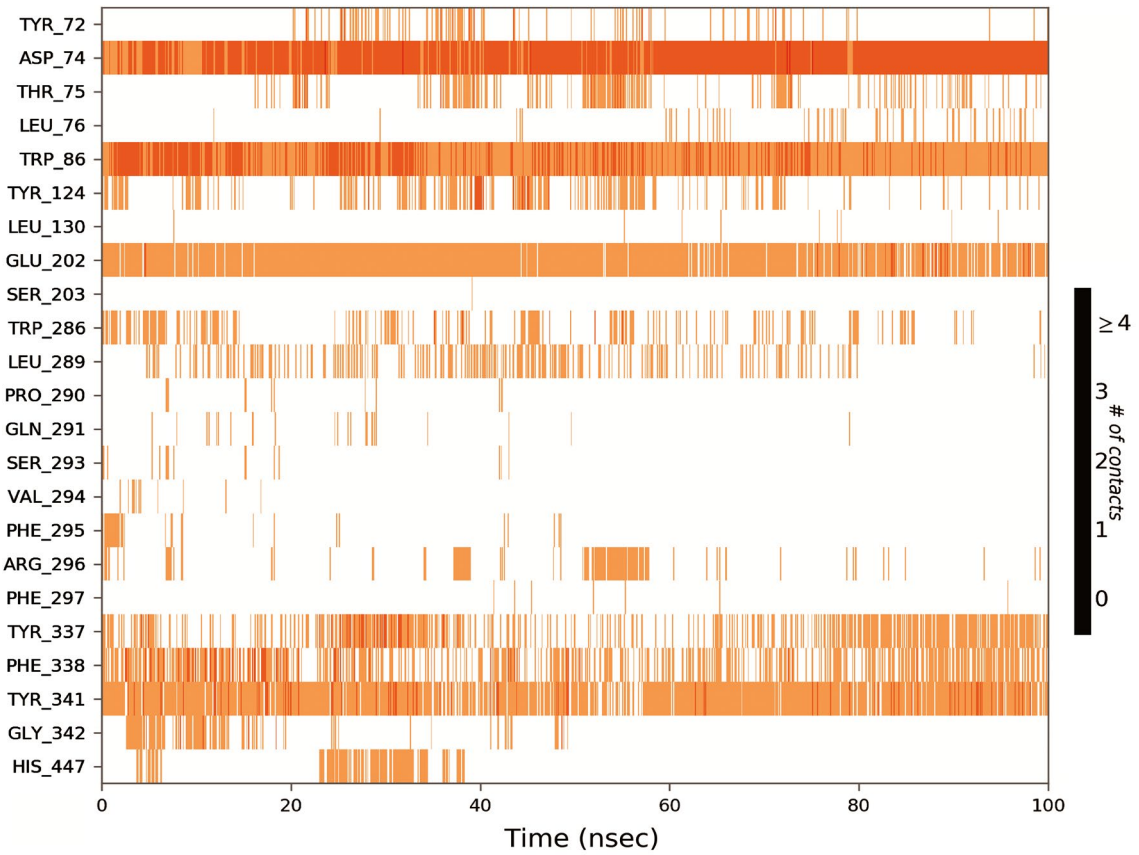


**Fig. 9** A timeline representation for 100 ns simulation run analysis of JFD03947 and AChE docked complex

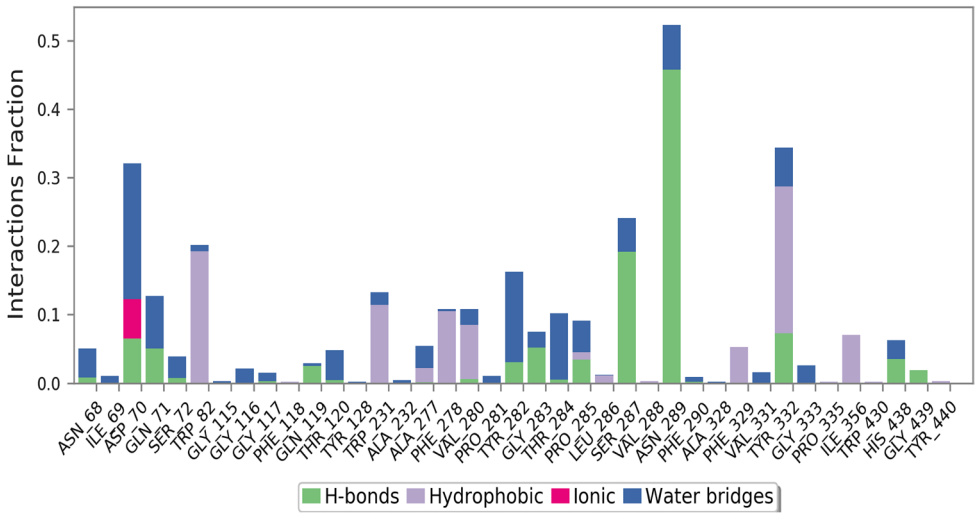


**Fig. 10** Stacked bar chart representation of JFD03947 with active site amino acid residues of BChE

HTS040889) obtained after virtual screening showed lesser MM/GBSA values than JFD03947. In the MD simulation study, their trajectories and binding stability in the CAS, PAS, and Anionic sub-site of AChE and BChE targets were also found to be unstable during the whole simulation time. Trajectories of other hits (AW00308, HTS040889) show more significant fluctuations in AChE and not found to be acceptable regions in the BChE. These preceding findings have prompted us to select JFD03947 as a potential hit.

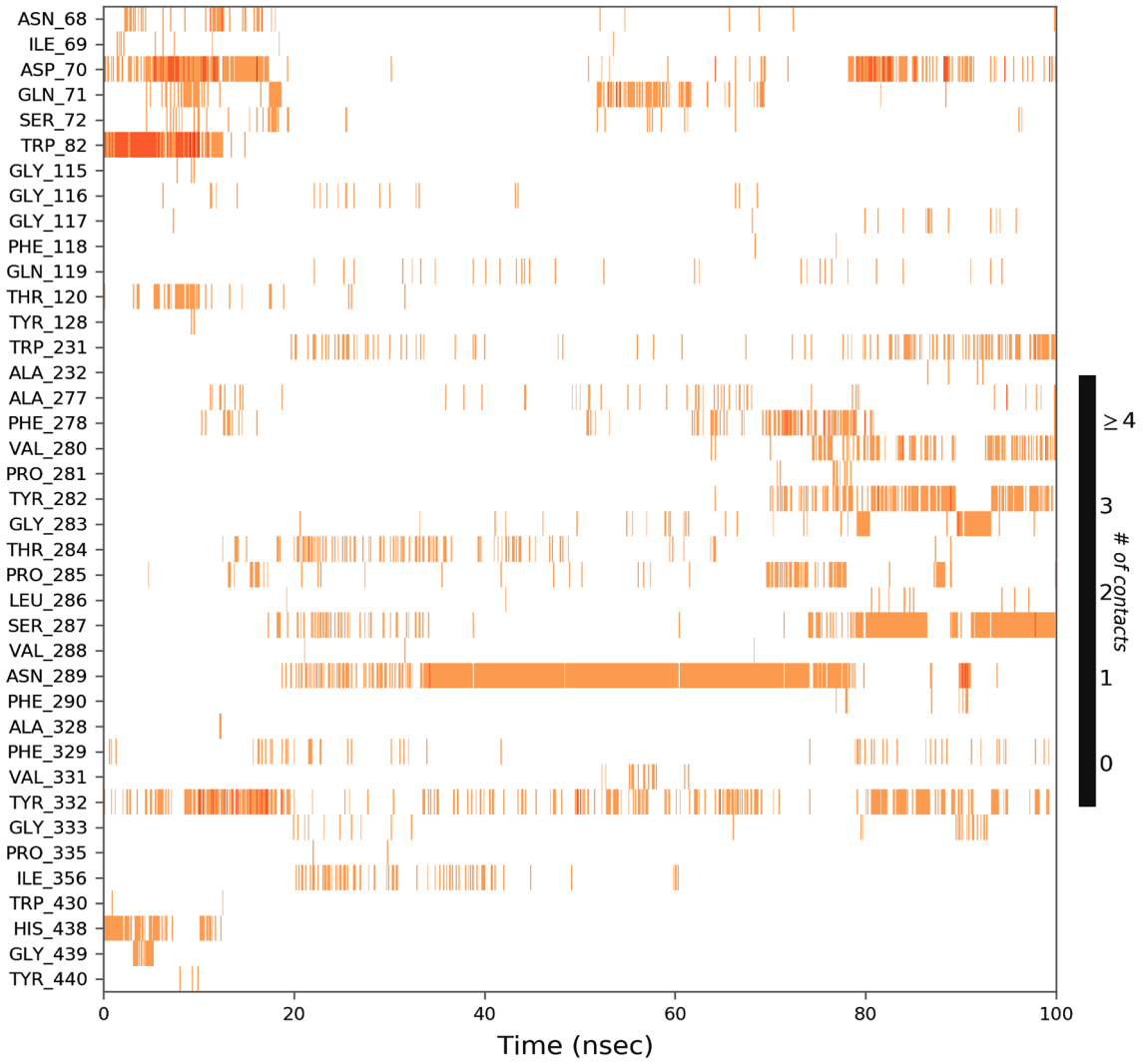


**Fig. 11** A timeline representation for 100 ns simulation run analysis of JFD03947 and BChE docked complex.

## Chemistry: synthesis and spectral characterization

The compound (JFD03947) was synthesized by the nucleophilic addition of amino group (nucleophile) of 1,4-bis(aminomethyl)cyclohexane (cis- and trans- mixture) (**1**) on carbonyl group (>C=O) of 2-hydroxybenzaldehyde (**2**) to form an unstable amino methanol intermediate that generated an imine (JFD03947) after dehydration (Scheme 1). The preliminary identification of imine was confirmed by a positive dragendorff test on TLC (Thin layer chromatography). The FT-IR of the synthesized compound showed a diagnostic stretching of (>C=N) imine group at

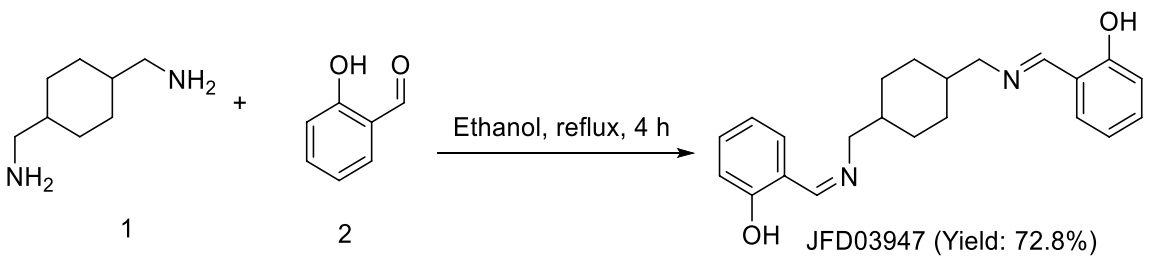


**Scheme 1** Synthesis of JFD03947

1606 $cm^{-1,}$ and the phenolic hydroxyl (OH) group exhibited a broad stretching at 3460 $cm^{-1}$. $^{1}H$ NMR spectrum of compound JFD03947 showed the appearance of a characteristic peak of imine proton (N=C**H**) at 8.53 ppm and also observed the disappearance of aldehydic (–C**H**O) proton. The phenolic hydroxyl group (Ph-O**H**) found at 13.75 ppm. $^{13}C$ NMR spectrum showed a distinctive peak of 166.36 ppm (>**C**=N–) and, 161.42 ppm (Ph–**1C**–OH). These spectral data confirmed the hypothesis of the reaction and formation of the compound (JFD03947). The result of the elemental analysis was also found within the range of ± 0.4% of theoretical values.

## In vitro biological evaluation

### Cholinesterase (hAChE and hBChE) inhibition assay

The $IC_{50}$ values and inhibitory potential of synthesized compound (JFD03947) and standard (donepezil and rivastigmine) against hAChE and hBChE were determined by the Ellman method. In vitro Ellman assay showed that JFD03947 significantly inhibited hAChE ($IC_{50}$ = 0.062 µM) as well as hBChE, ($IC_{50}$ = 1.482 µM). The obtained hAChE inhibitory potential was comparable to standard donepezil (hAChE, $IC_{50}$ = 0.040 µM), a selective AChE inhibitor, while BChE inhibitory potential was observed to slightly lower than selective BChE inhibitor, i.e., rivastigmine (hBChE, $IC_{50}$ = 0.864 µM) (Table 3). The obtained results of inhibition assay also validated the outcome of in silico study with JFD03947 being the potent compound interacting significantly with PAS and CAS residues of both cholinesterases.

To gain further insights into the mechanism of inhibition by JFD03947, enzyme kinetics study was performed against hAChE and hBChE. The type of inhibition was elucidated by the Lineweaver-Burk double reciprocal plot between the initial velocity of the substrate (y-axis) at increasing concentrations (x-axis; acetylthiocholine iodide for hAChE; butyrylthiocholine iodide for hBChE). The plots revealed decreased $V_{max}$, while $K_m$ increased with increasing concentration of JFD03947, the trend being attributed to the mixed-type of inhibition for hAChE and hBChE (Figs. 12a and 13a). The Dixon plots were constructed between Lineweaver-Burk slope and inhibitor concentration (Figs. 12b and 13b). The intersection point at the x-axis of the plot considered as dissociation constant $K_i$ for the inhibitor, which was estimated to be 0.036 µM and 1.2 µM for hAChE and hBChE, respectively.

**Table 3** In vitro inhibition assay results of screened compound JFD03947 and standard (Donepezil and Rivastigmine)

| S. no. | Compound | $IC_{50}$ (µM) ± SEM | | Selectivity Index |
|---|---|---|---|---|
| | | **hAChE** | **hBChE** | |
| 1. | JFD03947 | 0.062 ± 0.003 | 1.482 ± 0.071 | 23.90 |
| 2. | Donepezil | 0.040 ± 0.002 | 4.820 ± 0.124 | 120.5 |
| 3. | Rivastigmine | 1.682 ± 0.082 | 0.864 ± 0.046 | 0.513 |

All the results are reported as $IC_{50}$ ± SEM of at least three separate experiments

[a]SI (Selectivity Index) = $IC_{50}$ of BChE/$IC_{50}$ of AChE

### Aβ aggregation inhibition by thioflavin T assay

Accumulation and aggregation of Aβ peptide in the CNS regions of the brain is a significant detrimental cause of AD. The thioflavin-T assay was performed to evaluate the disaggregation potential of compound JFD03947. The experiment was conducted at three different concentration ratios of Aβ and inhibitor (10:5 µM, 10:10 µM, and 10:20 µM, respectively). The results were reported as NFI and % Aβ aggregation inhibition. The inhibitory potential of the compound was dependent on inhibitor concentration, and higher concentration inhibits maximum (Fig. 14a, b). The results revealed that the inhibitory potential of compound JFD0394 (NFI: 0.55–0.81), (% Aβ aggregation inhibition: 36–73%), was significantly higher than donepezil (NFI: 0.25–0.64) (% Aβ aggregation inhibition: 30–52%). The results of the Aβ inhibition assay were corroborated with the in-silico study.

### Neuroprotection studies on SH-SY5Y cell line

The neuroprotective activity was determined against human neuroblastoma SH-SY5Y cell lines using 3-(4,5-dimethylthiazol-2-yl)-2,5-diphenyl tetrazolium bromide (MTT) assay. The activity was performed using four different concentrations of test compounds in the range of 10–80 µM to determine their potential to prevent cell death against Aβ-induced oxidative stress. In this assay, 20 µM of Aβ was incubated with SH-SY5Y cells to attenuate % cell viability to 58% compared to control (Fig. 15). The results demonstrated augmented cell viability from 70 to 89% by the compound in a dose-dependent manner. The obtained result suggested the neuroprotective activity of compound JFD03947 towards SH-SY5Y neuroblastoma cell lines against the Aβ-induced oxidative stress.

## Discussion

The multifactorial nature of Alzheimer's disease and continued failure of the clinical candidate creates a need to explore the drugs which could act as multi-target therapeutics against Alzheimer's disease [49]. The present work is focused on the computational identification of a potent lead molecule against AD. Donepezil is a second-generation cholinesterase inhibitor widely used for the treatment of AD disease [50].

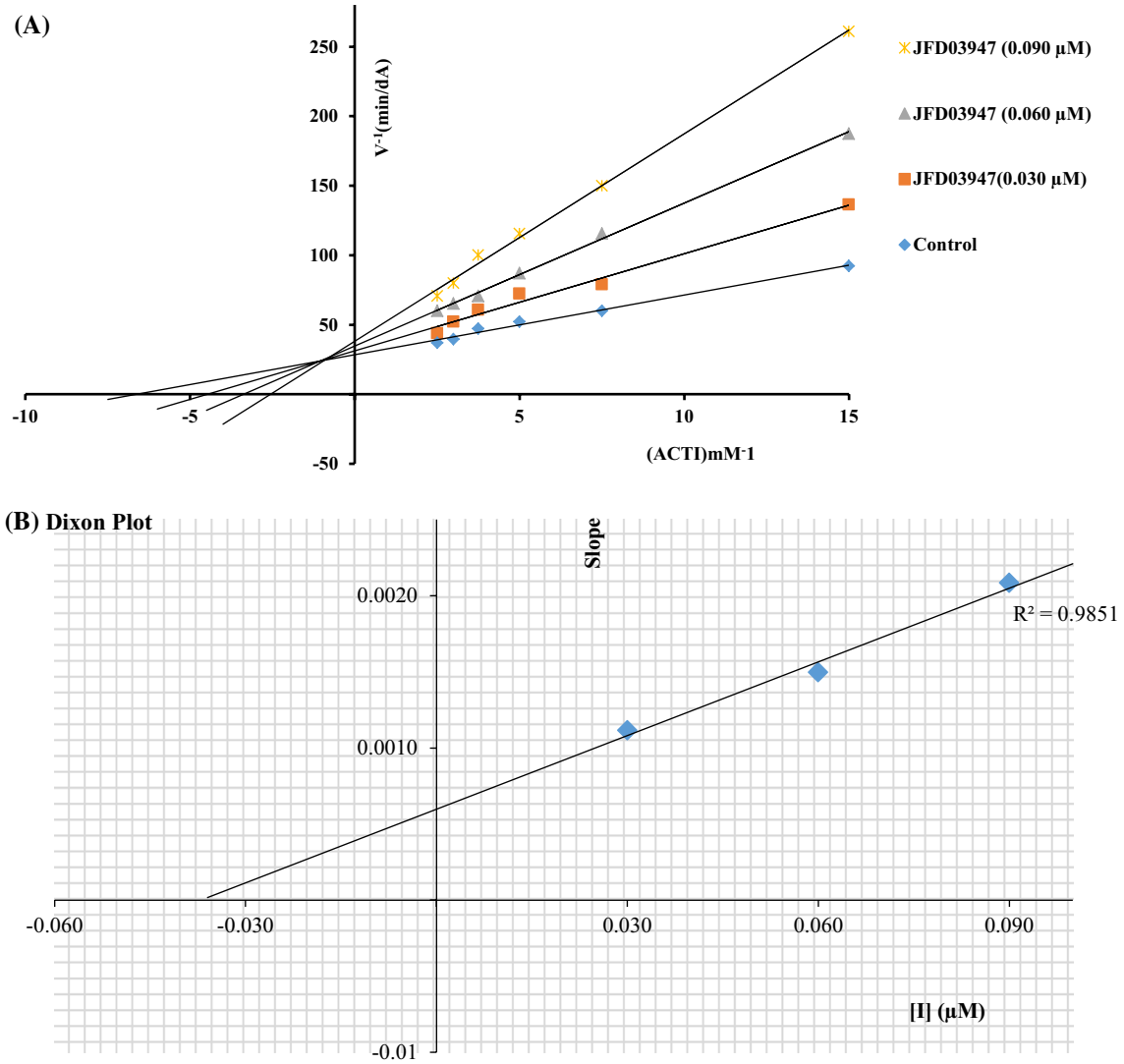


**Fig. 12** Enzyme kinetics study of JFD03947 against hAChE showing mixed type of inhibition; **a** Lineweaver–Burk plot. **b** Dixon plot

Donepezil acts as a reversible inhibitor and is used for the mild to severe cases of AD and readily cross the blood–brain barrier permeability to inhibit the AChE in the central nervous system [51, 52]. Donepezil occupies and binds equally well in the anionic binding site PAS, the acyl pocket, and the catalytic site CAS by adopting their outward–inward–inward orientations regardless of the substrate occupancy [53]. Rivastigmine, a reversible cholinesterase inhibitor, has higher selectivity toward the BChE and is used for the treatment of mild to moderate Alzheimer's disease [54].

The docking study of JFD03947 on AChE revealed similar CAS binding site interactions similar to donepezil. Whereas, at acyl binding pocket, o-hydroxy benzylidine moiety formed hydrophobic interaction identical to the 1H-inden-1-one moiety of donepezil. The anionic subsite and PAS region were also found to show the same interaction pattern.

Further, molecular dynamics simulation studies of the JFD03947-AChE docked complex revealed the similar RMSD trajectories and stability behavior like the donepezil-AChE docked complex during the simulation time. The docked pose of JFD03947 at BChE revealed that it showed the charged interaction with the CAS site similar to the rivastigmine. At the PAS site, it was observed that JFD03947 showed the hydrophobic interaction and salt bridge interaction identical to the rivastigmine. Anionic subsite interaction was also found similarities with the rivastigmine.

The dynamics simulations of the JFD03947-BChE docked complex showed the same stability and fluctuating behavior comparable to the rivastigmine, while the other docked complexes were found to show their unstable behavior during the simulation studies. Thus, results suggested JFD03947 as a potential inhibitor acting on AChE and BChE with a similar mode of interaction pattern and comparable

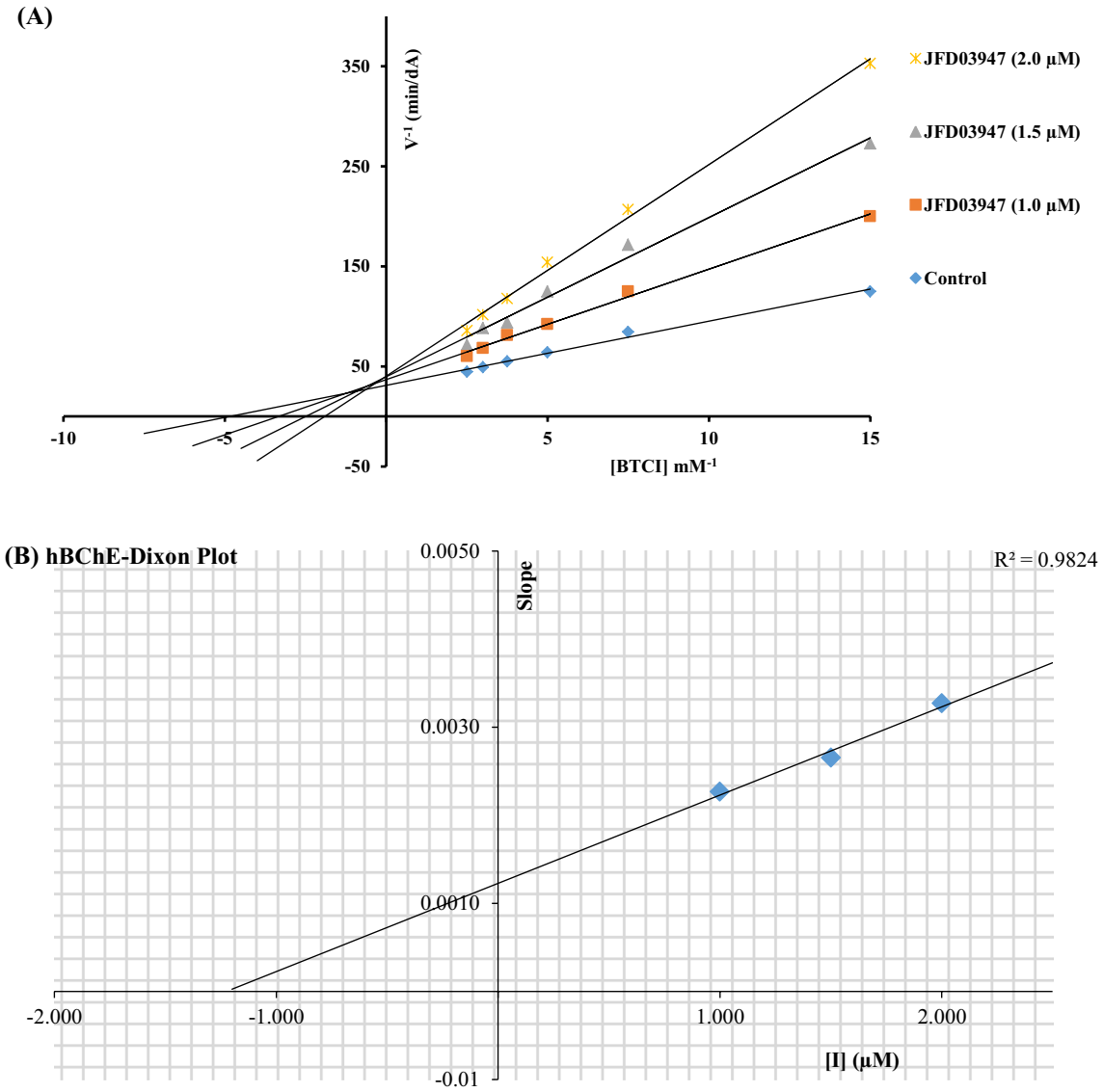


**Fig. 13** Enzyme kinetics study of JFD03947 against hBChE showing mixed type of inhibition; **a** Lineweaver–Burk plot. **b** Dixon plot

stability and fluctuation behaviors like donepezil and rivastigmine, respectively. Donepezil is more selective towards AChE, while rivastigmine has higher selectivity in inhibiting BChE [55]. Further, in vitro results showed that JFD03947 inhibited hAChE with an $IC_{50}$ value of 0.062 µM and hBChE with an $IC_{50}$ value of 1.482 µM. The substantial inhibition of AChE and BChE with the treatment of JFD03947, which has dimethenamine moiety, supports the fact of previous studies about choline esterase inhibitor.

The $IC_{50}$ value of the identified compound JFD03947 showed better results in the micromolar ranges as compared to the dimethylamine derivatives, which showed an $IC_{50}$ value of 1.83 µM for AChE [56]. The identified compound JFD03947 has also shown better activity in the micromolar range as compared to the compounds which have benzamide and picolinamide moiety containing dimethylamine side chain [57]. Thus, JFD03947 has shown potential activity and inhibition as compared to previously designed compounds containing dimethenamine moiety. To identify the mechanism of inhibition by the JFD03947, an enzyme kinetics study was performed, and the results elicited its mixed-type of inhibition against the hAChE and hBChE.

Further, thioflavin T assay also established its potential to prevent the Aβ aggregation apart from its cholinergic activity. JFD03947 was also found to be devoid of neurotoxic liabilities against SH-SY5Y neuroblastoma cell lines study. Based on the study, we conclude that the present study encompasses the identification of preliminary scaffold targeting on both cholinesterases, which will be further used

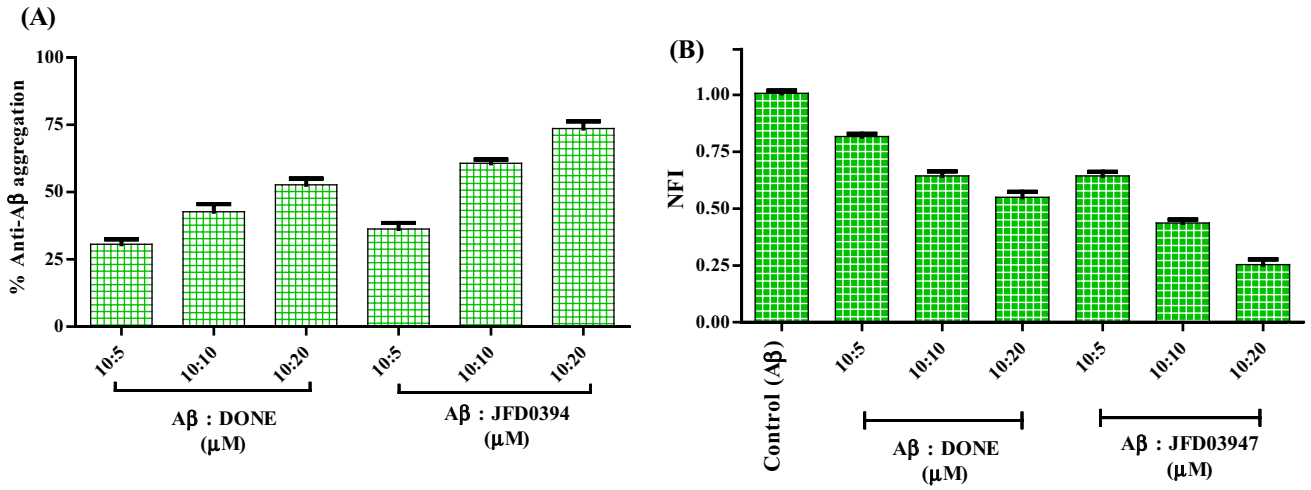


**Fig. 14** Result of thioflavin T assay by JFD03947 **a** % Aβ aggregation inhibition, **b** NFI. All the data are represented as mean ± SEM of three independent experiments (n = 3); *DONE* donepezil

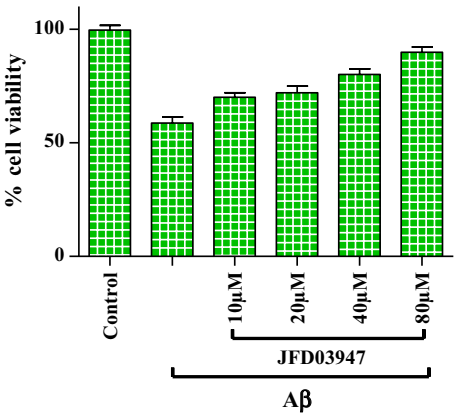


**Fig. 15** Neuroprotective activity of JFD03947 against Aβ-induced oxidative stress in SH-SY5Y cell lines by MTT assay. Each bar displays the values of % cell viability as the mean ± SEM of three separate experiments (n = 3).

to optimized chemically using molecular hybridization or bioisosterism approaches to get more significant results.

## Conclusion

Computational exploration of the database yielded significantly potential hit JFD03947 with stable and active binding site interactions against AChE and BChE. Virtual screening protocols were employed to screen the ligands initially from the Maybridge database of 14,400 compounds (18,930 generated conformers). Docking-post processing and pose filtration protocols were initiated to identify three potential hits (AW00308, HTS04089, and JFD03947) interacting effectively with both targets (AChE and BChE). These potential hits were processed for MM-GBSA, and molecular dynamics simulations to identify the best hit (JFD03947). The preceding findings of in silico computational studies have encouraged us to synthesize, characterize, and evaluate the best hit JFD03947 against cholinesterases (hAChE and hBChE) by in vitro Ellman assay. The molecule was obtained by single-step synthesis and resulted in good yield and also suggested the low production cost of the synthesized compound. The experimental results showed that JFD03947 inhibits hAChE with an $IC_{50}$ value of 0.062 μM and hBChE with an $IC_{50}$ value of 1.482 μM. Further, biological evaluations indicated that JFD03947 showed potential activity against Aβ aggregation as well as significant neuroprotective activity towards SH-SY5Y neuroblastoma cell lines. The findings of in vitro assays showed that identified hit JFD03947 elicited dual inhibitory potential against both cholinesterases and Aβ aggregation, which were also concurrent with the in silico findings. The overall results advocated that JFD03947 could be considered as a promising lead and further utilized to design a series of derivatives that could be explored to target multiple pathways of the AD.

**Acknowledgments** The authors gratefully acknowledge to Indian Institute of Technology (BHU) for providing financial assistance through postdoctoral fellowship (Grant No. PDF/007/15-16/16-17). The authors are also thankful to the Department of Health Research, Ministry of Health and Family Welfare for providing the Young Scientist Project in newer areas of Drugs Chemistry (DHR/HRD/YS-15-2015-16).

## References

1. Albert MS, DeKosky ST, Dickson D, Dubois B, Feldman HH, Fox NC, Gamst A, Holtzman DM, Jagust WJ, Petersen RC (2011) Alzheimer's Dementia 7(3):270

2. Darras FH, Pockes S, Huang G, Wehle S, Strasser A, Wittmann H-J, Nimczick M, Sotriffer CA, Decker M (2014) ACS Chem Neurosci 5(3):225
3. Sharma P, Tripathi A, Tripathi PN, Prajapati SK, Seth A, Tripathi MK, Srivastava P, Tiwari V, Krishnamurthy S, Shrivastava SK (2019) Eur J Med Chem 167:510
4. Wilson RS, Leurgans SE, Boyle PA, Bennett DA (2011) Arch Neurol 68(3):351
5. Tripathi PN, Srivastava P, Sharma P, Tripathi MK, Seth A, Tripathi A, Rai SN, Singh SP, Shrivastava SK (2019) Bioorg Chem 85:82
6. Klimova B, Maresova P, Valis M, Hort J, Kuca K (2015) Clin Interv Aging 10:1401
7. Shrivastava SK, Sinha SK, Srivastava P, Tripathi PN, Sharma P, Tripathi MK, Tripathi A, Choubey PK, Waiker DK, Aggarwal LM (2019) Bioorg Chem 82:211
8. Kalaria RN, Maestre GE, Arizaga R, Friedland RP, Galasko D, Hall K, Luchsinger JA, Ogunniyi A, Perry EK, Potocnik F (2008) Lancet Neurol 7(9):812
9. Iqbal K, Grundke-Iqbal I (2010) Alzheimer's disease, a multifactorial disorder seeking multitherapies. Elsevier, New York
10. Sharma P, Tripathi A, Tripathi PN, Singh SS, Singh SP, Shrivastava SK (2019) ACS Chem Neurosci 10(10):4361
11. Ferreira Neto DC, Alencar Lima J, Sobreiro Francisco Diz de Almeida J, Costa França TC, Jorge do Nascimento C, Figueroa Villar JD (2018) J Biomol Struct Dyn 36(15):4099
12. Mishra P, Sharma P, Tripathi PN, Gupta SK, Srivastava P, Seth A, Tripathi A, Krishnamurthy S, Shrivastava SK (2019) Bioorg Chem 89:103025
13. Tripathi PN, Srivastava P, Sharma P, Seth A, Shrivastava SK (2019) Biorg Med Chem 27(7):1327
14. Xu Y, Cheng S, Sussman JL, Silman I, Jiang H (2017) Molecules 22(8):1324
15. Srivastava P, Tripathi PN, Sharma P, Rai SN, Singh SP, Srivastava RK, Shankar S, Shrivastava SK (2019) Eur J Med Chem 163:116
16. Srivastava P, Tripathi PN, Sharma P, Shrivastava SK (2019) Biorg Med Chem 27(16):3650
17. Tripathi A, Choubey PK, Sharma P, Seth A, Saraf P, Shrivastava SK (2020) Bioorg Chem 95:103506
18. Sharma P, Tripathi MK, Shrivastava SK (2020) Cholinesterase as a target for drug development in Alzheimer's disease. Methods Mol Biol 2089:257–286
19. Schelterns P, Feldman H (2003) Lancet Neurol 2(9):539
20. Eskander MF, Nagykery NG, Leung EY, Khelghati B, Geula C (2005) Brain Res 1060(1–2):144
21. Santarpia L, Grandone I, Contaldo F, Pasanisi F (2013) J Cachexia Sarcopenia Muscle 4(1):31
22. Hartmann J, Kiewert C, Duysen EG, Lockridge O, Greig NH, Klein J (2007) J Neurochem 100(5):1421
23. Manoharan I, Boopathy R, Darvesh S, Lockridge O (2007) Clin Chim Acta 378(1–2):128
24. Greig NH, Utsuki T, Yu Q-s, Zhu X, Holloway HW, Perry T, Lee B, Ingram DK, Lahiri DK (2001) Curr Med Res Opin 17(3):159
25. Lane RM, Potkin SG, Enz A (2006) Int J Neuropsychopharmacol 9(1):101
26. Perry EK, Perry R, Blessed G, Tomlinson B (1978) Neuropathol Appl Neurobiol 4(4):273
27. Bullock R, Lane R (2007) Curr Alzheimer Res 4(3):277
28. Sharma P, Srivastava P, Seth A, Tripathi PN, Banerjee AG, Shrivastava SK (2019) Prog Neurobiol 174:53
29. Smith MA, Rottkamp CA, Nunomura A, Raina AK, Perry G (2000) Biochim Biophys Acta (BBA). Basis of Disease 1502(1):139
30. Inestrosa NC, Dinamarca MC, Alvarez A (2008) FEBS J 275(4):625
31. Inestrosa NC, Alvarez A, Perez CA, Moreno RD, Vicente M, Linker C, Casanueva OI, Soto C, Garrido J (1996) Neuron 16(4):881
32. Sastry GM, Adzhigirey M, Day T, Annabhimoju R, Sherman W (2013) J Comput Aided Mol Des 27(3):221
33. Shivakumar D, Williams J, Wu Y, Damm W, Shelley J, Sherman W (2010) J Chem Theory Comput 6(5):1509
34. Friesner RA, Murphy RB, Repasky MP, Frye LL, Greenwood JR, Halgren TA, Sanschagrin PC, Mainz DT (2006) J Med Chem 49(21):6177
35. Jacobson MP, Pincus DL, Rapp CS, Day TJ, Honig B, Shaw DE, Friesner RA (2004) Proteins 55(2):351
36. MacKerell AD Jr, Bashford D, Bellott M, Dunbrack RL Jr, Evanseck JD, Field MJ, Fischer S, Gao J, Guo H, Ha S (1998) J Phys Chem B 102(18):3586
37. Heindel ND, Lemke SM, Fish VB (1967) J Chem Eng Data 12(4):596
38. Ellman GL, Courtney KD, Andres V Jr, Featherstone RM (1961) Biochem Pharmacol 7(2):88
39. Peauger L, Azzouz R, Gembus V, Tintas M-L, Sopková-de Oliveira Santos J, Bohn P, Papamicaël C, Levacher V (2017) J Med Chem 60(13):5909
40. Lineweaver H, Burk D (1934) J Am Chem Soc 56(3):658
41. Dixon M (1972) Biochem J 129(1):197
42. Levine IIIH (1993) Protein Sci 2(3):404
43. More SS, Vince R (2012) ACS Chem Neurosci 3(3):204
44. Kontoyianni M, McClellan LM, Sokol GS (2004) J Med Chem 47(3):558
45. Wang R, Lu Y, Wang S (2003) J Med Chem 46(12):2287
46. Kryger G, Silman I, Sussman JL (1999) Structure 7(3):297
47. Cheung J, Rudolph MJ, Burshteyn F, Cassidy MS, Gary EN, Love J, Franklin MC, Height JJ (2012) J Med Chem 55(22):10282
48. Dighe SN, De la Mora E, Chan S, Kantham S, McColl G, Miles JA, Veliyath SK, Sreenivas BY, Nassar ZD, Silman I (2019) Commun Chem 2(1):1
49. Carmo Carreiras M, Mendes E, Jesus Perry M, Paula Francisco A, Marco-Contelles J (2013) Curr Top Med Chem 13(15):1745
50. Cacabelos R (2007) Neuropsychiatr Dis Treat 3(3):303
51. Agatonovic-Kustrin S, Kettle C, Morton DW (2018) Biomed Pharmacother 106:553
52. Goodman LS (1996) Goodman and Gilman's the pharmacological basis of therapeutics. McGraw-Hill, New York
53. Silva MA, Kiametis AS, Treptow W (2020). J Chem Inf Model. https://doi.org/10.1021/acs.jcim.9b01073
54. Schneider LS (2000) Dialogues Clin Neurosci 2(2):111
55. Kandiah N, Pai M-C, Senanarong V, Looi I, Ampil E, Park KW, Karanam AK, Christopher S (2017) Clin Interv Aging 12:697
56. Luo W, Su Y-B, Hong C, Tian R-G, Su L-P, Wang Y-Q, Li Y, Yue J-J, Wang C-J (2013) Bioorg Med Chem 21(23):7275
57. Gao X-h, Liu L-b, Liu H-r, Tang J-j, Kang L, Wu H, Cui P, Yan J (2018) J Enzyme Inhib Med Chem 33(1):110